Under-ice acoustic navigation using real-time model-aided range estimation

EeShan C. Bhatt,[1,2,a] Oscar Viquez,[2] and Henrik Schmidt[2,b]

[1]*MIT-WHOI Joint Program in Oceanography/Applied Ocean Science & Engineering,*

Cambridge and Woods Hole, MA, USA

[2]*Department of Mechanical Engineering, Massachusetts Institute of Technology,*

Cambridge, MA

(Dated: 21 December 2021)

The long baseline (LBL) underwater navigation paradigm relies on the conversion of recorded travel time to range to trilaterate for position. For real-time navigation, this conversion assumes an isovelocity sound speed. For re-navigation in post-processing, computationally and/or labor intensive acoustic modeling may be employed to reduce uncertainty driven by multipath arrivals. This work demonstrates an embedded, ray-based prediction method of the effective horizontal group speed to minimize vehicle position error. This method was implemented for a small scale AUV-LBL system in March 2020, in the Beaufort Sea, in total under-ice conditions and a double ducted acoustic propagation environment. The vehicle was successfully deployed and recovered. Given the lack of GPS data throughout the vehicle's mission, however, the localization performance is quantified between GPS-linked beacon-to-beacon connections where a single beacon ran the vehicle's navigation stack. The real-time positioning error is roughly 11 meters at distances up to 3 km. In post-processing, the dataset is extended to all possible beacon-to-beacon events. The localization performance is reevaluated with an operationally equivalent navigation stack using modeled, historical, and locally observed sound speed profiles for a Minimal Bounce Criteria (MBC), as deployed in real-time, and an improved algorithm, the Nearest Bounce Criteria (NBC). The best performing median re-positioning errors are roughly 10 and 2 meters, respectively. Further investigation suggests that the GPS ground truth data have some noise that is not reciprocated in the travel time data.

[a]ebhatt@whoi.edu

[b]henrik@mit.edu

I. INTRODUCTION

Autonomous underwater vehicles (AUVs) are increasingly capable platforms to explore and sample the ocean, particularly for remote and/or dangerous regions. However, navigation uncertainty is a major challenge in considering AUVs as standard tools for oceanographic research. While land and air-based robots utilize information from Global Positioning System (GPS) updates—or more broadly, any Global Navigation Satellite System (GNSS)—to achieve stunning location accuracy and precision throughout the duration of their missions, AUVs cannot access GPS while underwater due to the rapid attenuation of electromagnetic waves. Therefore, underwater vehicle navigation has relied on any combination of dead reckoning, hydrodynamic models, inertial navigation systems, doppler velocity logs, and acoustic baseline positioning systems (Paull *et al.*, 2014). Limiting navigation error and drift requires an AUV to periodically stall on the surface and obtain a GPS fix to reset its position error. This foolproof method of self-positioning is undesirable for stealth, adverse weather conditions, and mission efficiency, and inaccessible in a GPS-denied situation like an ice-covered environment.

Of acoustic baseline positioning systems, long baseline (LBL) is the most GPS-like in style and scale, and most appropriate for mitigating drift in underwater vehicle localization without overburdening computation or payload size on the vehicle (Paull *et al.*, 2014; Van Uffelen, 2021). The state-of-the-art for LBL assumes an isovelocity, linear scaling between one way travel time (OWTT) and range (Eustice *et al.*, 2006, 2007; Webster *et al.*, 2009, 2012). This assumption is valid for short scale operations but introduces error for complex acoustic

propagation environments. Thus, this paper demonstrates embedded acoustic model-aided data processing to convert recorded OWTTs into pseudoranges. This approach was necessitated by a low risk tolerance for navigation error, given total under-ice conditions and double ducted acoustic environment, in the Beaufort Sea, in March 2020, during the Ice Exercise 2020 (ICEX20). We quantify the success of the proposed acoustic ranging method on GPS-linked beacon-to-beacon communication events, not the AUV-LBL positioning itself, as the latter has no ground truth GPS to compare to.

A. Timing, Positioning, and Navigation

In the interest of clarity, we formally reiterate definitions of timing, positioning, and navigation (CITE). Timing is the ability to maintain accurate and precise time synchronized across multiple nodes. Positioning is the ability to accurately determine one's location referenced to a standard geodetic system. It can be done via trilateration or triangulation. Navigation, implying a degree of autonomy, is the ability to distinguish between current and desired position, and apply necessary corrections to course, orientation, and/or speed to attain that desired position. Thus, navigation is also intrinsically real-time and is predicated on positioning, which is predicated on timing.

Given the computational and physical barriers of assessing position in real-time, we define post-processing counterparts—re-navigation and re-positioning—which may be supplemented by additional data, model output, and computationally or labor intensive algorithms.

B. Background on underwater navigation, re-navigation, and re-positioning

Navigation efforts are currently limited to small-scale deployments, and take advantage

of the advent of the WHOI micro-modem (Singh *et al.*, 2006) and synchronized chip scale

atomic clocks (Gardner and Collins, 2016). Short range (less than ten kilometers) navigation

efforts achieve minimal error with a nominal sound speed value (Eustice *et al.*, 2007; Kepper

et al., 2017; Webster *et al.*, 2009). At larger scales on the order of hundreds of kilometers,

a deterministic (Graupe *et al.*, 2019) or through-the-sensor (Webster *et al.*, 2015) value for

sound speed was used, but error remained in the hundreds of meters.

Of particular note are previous efforts in the Arctic.

The LBL system provides navigation aiding as position updates to correct for localization

drift and error.

It is important to note that post-processing localization efforts (re-navigation for a self-

determinedly moving object or re-positioning for a passively moving one), are often applied

for large-scale deployments to better account for spatial variability in the ocean state.

Recently, buoyancy gliders have been re-navigated by considering a temporally averaged

depth dependent SSP and CTD observations of...

A well known example of long range re-positioning are RAFOS drifters that record the

timestamps of the four strongest pings; transmit all data after mission completion; and are

manually localized with uncertainties of 1.5 to 4.5 km (CITE ROSSBY, DUDA).

Other re-positioning methods employ four-dimensional ocean models. Wu *et al.* (2019)

compares acoustic records with synthetic acoustic records computed through HYCOM

82 (Chassignet *et al.*, 2007). Mikhalevsky *et al.* (2020) introduces an impressive "cold start"

83 algorithm that isolates a specific ray path to find a representative group speed, re-positioning

84 a floating hydrophone array with an error of 85 m and a standard deviation of 32 m relative

85 to ground truth GPS data. Implementing these algorithms for navigation remains to be

86 seen.

C. Underwater positioning and navigation in the Arctic

88 Underwater navigation research is broadly motivated by acquiring GPS-like navigation

89 accuracy in GPS-denied conditions. The Arctic, while remote, is the perfect place to test

90 mature navigation technologies in real GPS-denied conditions.

91 We refer the reader to excellent reviews of vehicle operations in the Arctic by Norgren

92 *et al.* (2014) and Barker *et al.* (2020). Previous AUV deployments in the Arctic (Bellingham

93 *et al.*, 1993) Literature and historical reviews of underwater navigation approaches in under-

94 ice conditions highlight the emerging technology learning curve for vehicle operations in the

95 Arctic, the hostile conditions brought on by a semi-permanent moving ice cover, and the

96 need for both absolute and relative navigation with little to no tolerance for error (Barker

97 *et al.*, 2020; McFarlane and Mackay, 2015; Norgren *et al.*, 2014).

98 One of the first successful AUV launches and recoveries involved equipping the vehicle

99 with barbs which became entangled into a homing net underneath the ice (Bellingham *et al.*,

100 1993). Since then, AUVs have been used for ocean bottom (Jakuba *et al.*, 2008; Kunz *et al.*,

101 2008), under-ice (Kaminski *et al.*, 2010), and hydrographic surveys (Kukulya *et al.*, 2016,

102 2010; Plueddemann *et al.*, 2012; Stevens *et al.*, 2016). These efforts show a combination

of short and long range positioning systems, where all acoustic navigation methods used a depth-averaged sound speed for linear scaling between recorded travel time and range. In many cases robust quantitative navigation performance could not be evaluated due to small operational scale and/or moving ice floes. But most importantly, all of these efforts experienced a nearly isovelocity or classical upward refracting Arctic acoustic environment.

The new Arctic—one with much less multi-year sea ice—is experiencing significant changes in the water column as well (MacKinnon *et al.*, 2021). The Beaufort Lens is a highly dynamic, highly stratified water mass, keeping a neutrally buoyant layer of warm Pacific water at 50 to 70 m in depth. Surrounded by cooler waters, it distinguishes a local maximum in the SSP, creating an upper and lower duct—the upper duct degrades signal coherence due to intensified ice interaction and the lower duct effectively traps sound for long range propagation (Poulsen and Schmidt, 2016). Modeling output (Duda *et al.*, 2021, 2019) and experimental observations (Badiey *et al.*, 2019; Ballard *et al.*, 2020; Kucukos-manoglu *et al.*, 2021) indicate a high degree of spatio-temporal variability of the lower duct throughout the Chukchki and Beaufort Seas.

An experiment in 2014 exploited this lower duct to provide acoustic navigation and communication at mesoscale ranges in the Canada Basin. Freitag *et al.* (2015) and Webster *et al.* (2015) deployed multiple GPS-linked ice buoys with transducers that were capable of communications greater than 400 km with a range accuracy of 40 m when the sound speed was known. The transducers were at 100 m depth, well-positioned in the lower duct spanning 50 to 200 m. The glider navigation accuracy, however, was severely degraded as acoustic packets were sent when the gliders were outside the sound channel. When gliders

125 were deployed again in 2017, their navigation error was on the order of half a kilometer, and

126 a glider re-navigation using an acoustic arrival method and the average sound-speed profile

127 from the gliders reduced navigation error by a factor of 4-5, depending on the dive (Graupe

128 *et al.*, 2019). Navigation error is referenced to intermittent GPS fixes, as all of these glider

129 deployments occurred in the Marginal Ice Zone with little to no ice at the time.

D. Ice Exercise 2020

131 During ICEX20, we deployed AUV *Macrura*, a custom Bluefin-21, in complete under-ice

132 conditions and a complex double ducted environment brought upon by a persistent warm

133 water intrusion in the Pacific Summer Water layer, which we call the Beaufort Lens. The

134 majority of the navigation updates were below 11 m and were small enough to enable an

135 emergency recovery. When considering operational variables such as range, vehicle class,

136 and propagation conditions, there are no comparable deployments.

137 The Beaufort Lens is equally important for shorter ranges as well, where a shadow zone

138 over vehicle operational ranges is created by a drastic change in the reliable acoustic path

139 (Schmidt and Schneider, 2016). Thus the key simplifying assumption for OWTT ranging—a

140 locally homogeneous sound speed profile that enables a linear, deterministic scaling between

141 travel time and range—becomes more inaccurate due to increased multipath in the upper

142 duct of the Beaufort Lens.

143 The results from this paper derive from data taken while deploying AUV Macrura, a

144 modified Bluefin-21, during the Ice Exercise 2020 (ICEX20), in the Beaufort Sea, in March

145 2020. The challenges anticipated for ICEX20—total ice cover, moving ice floes, and a vari-

able Beaufort Lens—crystallized the necessity of environmental awareness for the navigation solution.

In this paper we present a working solution for underwater navigation that achieves GPS-like accuracy and precision. We embed a stochastic prediction of a single group velocity to convert recorded travel time into range. This prediction ingests an updatable snapshot of the SSP via acoustic message; over the course of ICEX20, this capability was used several times. Ultimately, integrating environmental realism enabled a successful emergency recovery of the AUV. Due to a harddrive error, the AUV stalled underneath the ice surface and broadcasted its location. A team was able to dig a hole through the 2 meter ice sheet and immediately see the vehicle. Its successful recovery amidst total ice cover is shown in Fig. 1.

The rest of this paper is organized as follows: Section II presents the physical experimental setup and model-based data processing; section III quickly conveys real-time results and the limitations of the data collected; section IV presents key results for group velocity predictions and range estimations; section V closes with a discussion on importance, future work, and broader relevance.

II. METHODS

The acoustic communication dataset accrued for ICEX20 relied on the Integrated Communication and Navigation Network (ICNN) (Randeni *et al.*, 2020, 2021; Schneider *et al.*, 2020). The ICNN was initially developed via numerous virtual experiments, to push the boundaries of algorithms and interfaces between different hardware components. The simulation approach is a necessary testbed for robustness and produces better results than post-

FIG. 1. The successful emergency recovery of AUV Macrura, with the the auger used to drill through the ice sheet in the background. Photo courtesy of LT CDR D. Goodwin.

168 processing previous field data, as that restricts mission configurations to the data taken,

169 which can hamper troubleshooting in the field. The simulation capabilities are largely

170 physics-driven with a modular system of systems approach: an environmental simulator

171 with sub-components for the ocean, including Arctic ice drift and ocean acoustic propaga-

172 tion; a vehicle simulator with sub-components for vehicle dynamics and navigation; a topside

173 hardware simulator and acoustic communications simulator, both with a software-only con-

174 figuration and a hardware-in-the-loop version (Schneider and Schmidt, 2018). The virtual

175 environment similarly emulates the interfaces between the real components to test the entire

176 software pipeline. Both simulation capabilities are integral to mission success.

A. Operational paradigm on the ice

178 The ICNN is comprised of four ice buoys, in a loose rectangle, roughly 2 km away from

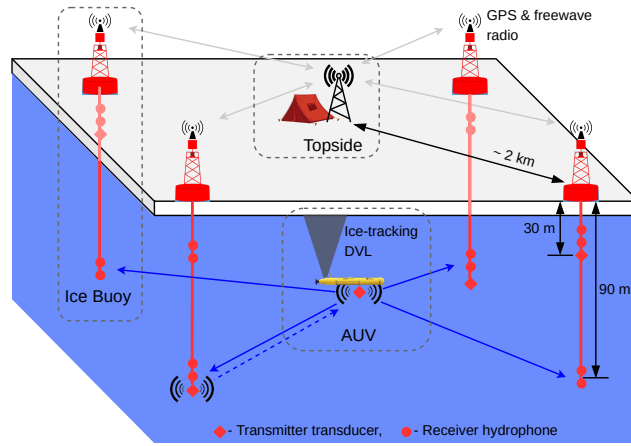179 a central ice camp with a topside computer, as shown in Fig. 2.

FIG. 2. A schematic overview of the Integrated Communication and Navigation Network (ICNN), which provides joint data-transfer and tracking between AUV and a human decision maker at Topside.

180 Each ice buoy is outfitted with a WHOI Micro-Modem (Singh *et al.*, 2006), with a four-

181 element receiver array and a single transmitter, and one-tenth of a millisecond resolution.

182 The receiving and transmitting elements were split between shallow and deeper depths (30

183 and 90 m, respectively) to provide better coverage due to the acoustic shadow zone in the

184 Beaufort Lens. The buoys do not encompass the full operating range of the vehicle but are

positioned to minimize overlap in trilateration for spherical positioning (Deffenbaugh *et al.*, 1996a).

Vehicle missions in any underwater environment, but especially acoustically complex ones, must balance competing uses of the acoustic channel. This network uses a single synchronized digital communication packet to provide both tracking and data to the operator. The ICNN operational paradigm is as follows:

1. The AUV, running an ice-tracking DVL and an onboard hydrodynamic model, broadcasts its perceived location on a scheduled, time-synchronized message via WHOI Micro-Modem

2. Four ice buoys, each outfitted with a WHOI Micro-Modem, receive messages from the AUV and send that information over freewave radio to a Topside computer

3. The topside computer converts travel times into range estimates using a stochastic embedded prediction of the horizontal group velocity via BELLHOP ray tracing code (Porter, 2011) coupled with a Virtual Ocean (Schneider and Schmidt, 2018)

4. The topside computer calculates a new position by trilaterating the range estimates

5. The position differential, not the absolute position, is broadcast to the vehicle to update its navigation solution and be robust to latency and intermittency

This paper specifically addresses the third step—the topside computer's conversion of travel time into range, which underpins the trilateration in the ICNN, and is an often overlooked element of any underwater acoustic navigation system. The analysis accordingly focuses on validating acoustic range estimates from communication events between GPS-

206 tracked beacons, not the AUV itself. This allows the results to be decoupled from all the

207 other moving parts in the ICNN. This "modem experiment" was conducted while the vehicle

208 was still being prepped to go under the ice.

B. Modem experiment design

210 Because the navigation solution on the vehicle during a mission can only be evaluated on

211 the basis of the error estimates sent, a sister experiment for validating the real-time ranging

212 approach was implemented. The ice buoy modems were run as "virtual vehicles" at a given

213 depth and would transmit to all other ice buoys. The internal sound speed estimate was

214 then toggled using a handful of weights applied to a basis function representation of the

215 sound speed. This trial was configured for as many ice buoy modems as possible with the

216 time allotted, with each experiment running for roughly an hour between the two sound

217 speed modalities. There are three important engineering choices in the ICNN network to

218 contextualize this dataset:

219 1. Each modem buoy only has one transmit depth layer (30 or 90 m)

220 2. The transmit and receive layers are independent

221 3. At any given time, the receive depth layers are the same across all four ice buoys

222 The design of the ICNN enables a self-adapting network to transmit and receive at the

223 optimal depth to maintain contact with the AUV (Schneider *et al.*, 2020). This adaptivity

224 was not used during the modem experiment but was instead toggled manually. Given

225 the complexity of the ICNN system, this experiment did not collect an exhaustive set of

data across all buoy, source depth, receive layer, and sound speed combinations, as this time was also used to verify and resolve any hardware issues in the modems themselves. Importantly, only one modem at a time could run the vehicle behavior to trigger group velocity calculations; other modems that were active during the experiment recorded events as tracking buoys, not as vehicles.

A key construction in the ICNN are parallel physical and virtual layers; given the small operational scale, on the order of kilometers, and a singular SSP, both layers are projected into a range independent coordinate system for ease of comparison. Furthermore, because one of the buoys was configured to act as a virtual vehicle at any given time during the modem experiment, the tracking range was supplemented with an additional modem deployed from the camp site and configured to act as a virtual buoy; the transducer attached to the camp site modem was lowered to a depth of 20 m.

1. Physical layer

The physical layer describes the acoustic link between beacons in the water column. It covers all source depths (20, 30, and 90 m) and both buoy receive layers (30 and 90 m), where the surface expressions of the beacons are tracked by GPS. Events are sorted by source depth and sound speed profile, given that these are the dominating factor for the location and span of the shadow zone compared to any temporal or spatial scales of variability.
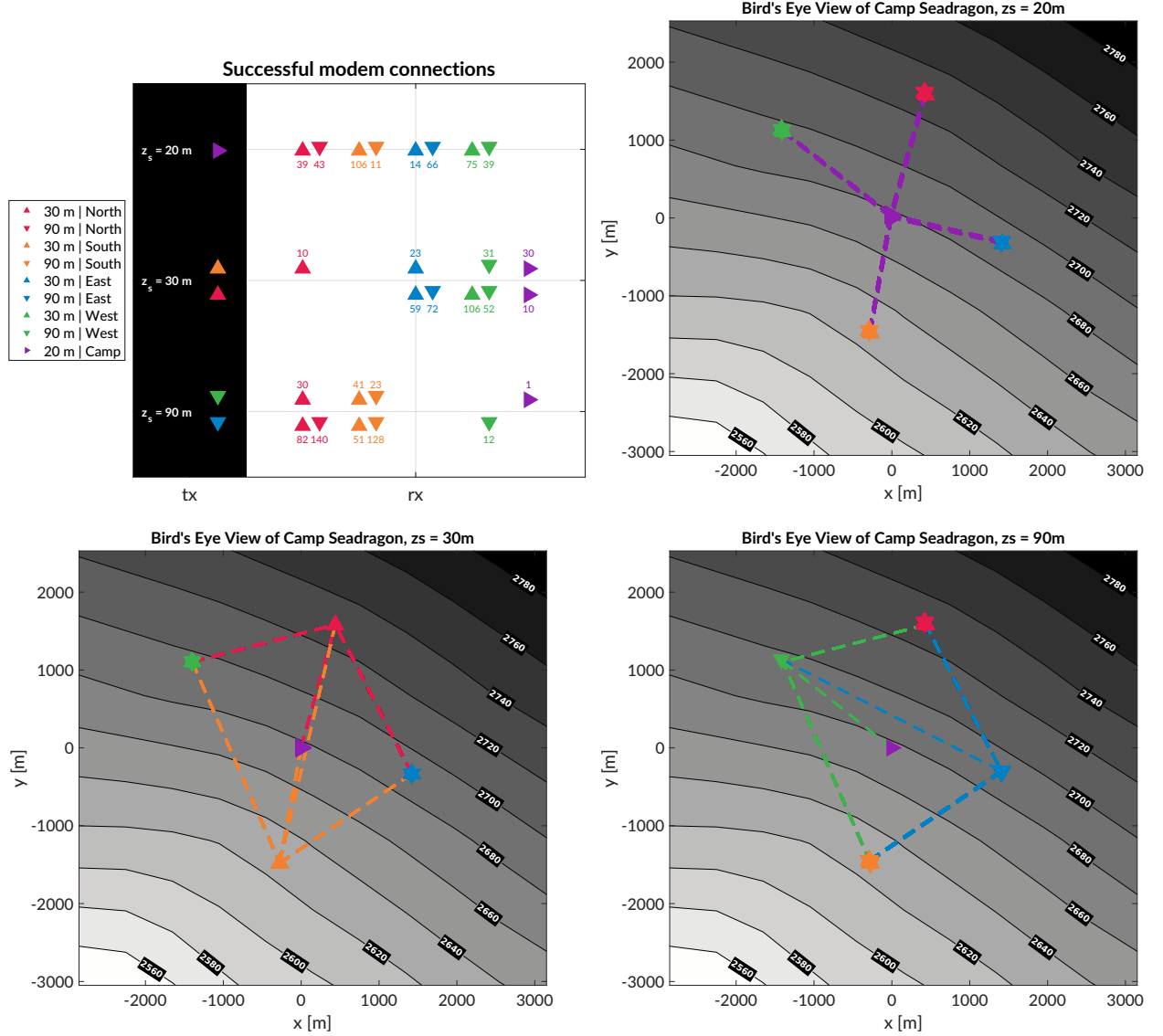
FIG. 3. An overview of the modem experiment by source and receiver depth and position. Subfigure

(a) shows a chart of the successful events between source and receiver depth. The black column

on the left, tx, shows the source depth, z_s. The column on the right, rx, shows the receivers

with the amount of good contacts. The orientation of the triangles—sideways, upwards, and

downwards—corresponds to depths of 20, 30, and 90 m. Subfigures (b-d) correspond to transmitter

depths of 20, 30, and 90 m, respectively. Topside, demarcated by the purple triangle, is situated

just north of the continental shelf.

²⁴⁴ **_2. Virtual layer_**

²⁴⁵ The virtual layer describes the BELLHOP simulations for each communication event in

²⁴⁶ the physical layer. The SSP used for the raytracing is driven by a handful of weights applied

²⁴⁷ to a basis function representation of the SSP variability to reconstitute a number of realistic

²⁴⁸ candidate SSPs (LeBlanc and Middleton, 1980; Lin _et al._, 2010). The SSP is the only human

²⁴⁹ configurable input to the group velocity prediction.

²⁵⁰ During ICEX20, the SSP was toggled between the historical "baseline" and a "weighted"

²⁵¹ estimate based on a local CTD cast, i.e. an optimal set of weights chosen by a human

²⁵² decision maker via an interactive Tactical Decision Aid framework (Bhatt _et al._, 2021). For

²⁵³ the post-processing analysis, we add the SSP from HYCOM for comparison, to mirror the

²⁵⁴ information available on a submarine—modeled data, historical data, and _in situ_ data (per-

²⁵⁵ sonal conversation with LT B. Howard and LT CDR D. Goodwin). This order corresponds

²⁵⁶ to increasing ducted conditions of the Beaufort Lens.

²⁵⁷ Fig. 4 shows eigenrays in a range independent coordinate system for all three sound speed

²⁵⁸ environments, for a source depth of 30 m. It is important to note that BELLHOP produces

²⁵⁹ an abundance of eigenrays; the ones displayed here are chosen by travel time proximity to

²⁶⁰ the recorded data. With this filter, the chosen eigenrays show a greater amount of surface

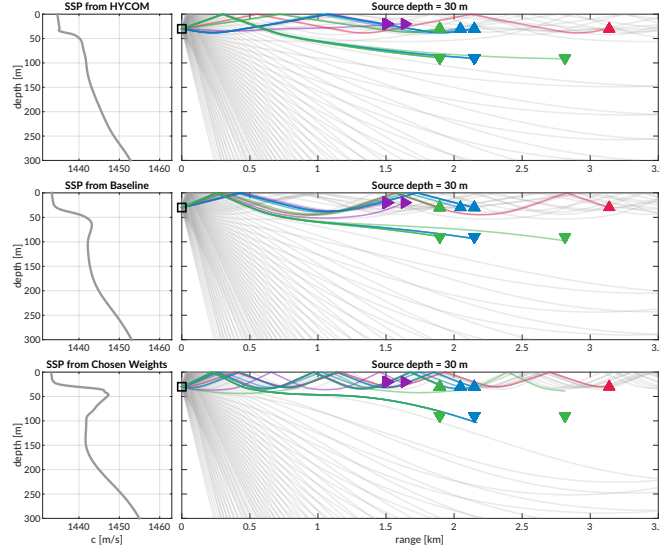²⁶¹ interactions as the SSP duct conditions increase.

FIG. 4. Eigenrays for beacon to beacon events for each sound speed with a nominal source depth of 30 m. The beacons are highlighted in color/marker coding in Fig. 3. The eigenrays are curated from BELLHOP by travel time proximity and are traced in the representative receiver colors over a total ray fan in gray.

C. Group velocity prediction methods

The variation of horizontal group velocity from any source-receiver pair is the fundamental challenge to implement GPS-like navigation in an LBL navigation paradigm, especially in an acoustically complex propagation environment. The use of the acoustic modem network for tracking relies on the accurate estimates of travel times between the submerged platform and range modems, supported by clock synchronization and a pre-determined scheduling of acoustic events. For the Beaufort Lens in particular, the strong multipath effects make it virtually impossible to deterministically predict the modem triggering time.

1. *Minimal bounce criteria (MBC)*

Instead, for each individual node i, an embedded stochastic tracking framework is used to provide a running estimate of the horizontal group velocity $u_{i,j}$ for the conversion from travel time to range from modem j, with the ultimate goal of matching the naive group velocity, i.e. the GPS-recorded distance between two nodes divided by the modem-recorded one way travel time between them.

In the ICEX20 configuration, the acoustic tracking is running on the topside computer, which controls the integrated communication and navigation range. Here we assume that the group velocities $u_{i,j}$ are smoothly varying over the course of a vehicle mission, i.e., with respect to range, mission time, and the frequency of updates relative to vehicle motion. The group velocity is continuously tracked using predictions from the *Virtual Ocean* infrastructure.

When the topside tracking framework receives a modem message, with a time delay, Δt, from one of the range modems, it will request a new estimate of the group velocity and its associated uncertainty. The group velocity estimate is found using the vehicle's reported depth and the extrapolated navigation solution for range, $\hat{r}$, as inputs for the ray tracing program. The latter returns an impulse response estimate in the form of ray travel times dt_j and amplitudes a_j for that range and depth.

The initial call to BELLHOP is over a sparse local grid, from which the plane wave approximation is used to interpolate the ray to the range and depth posited by the onboard tracking solution. For each grid point, BELLHOP will produce a number of arrivals resulting

291   from multiple propagation paths for any source-receiver pair. Using only the N_0 rays with

292   neither surface nor bottom bounces, it will then estimate the current group velocity u from

293   a power weighted average of the ray travel times,

$$u = \frac{\hat{r} \sum_{n=1}^{N_0} a_n^2}{\sum_{n=1}^{N_0} dt_n a_n^2} \ , \tag{1}$$

294   and the associated weighted standard deviation,

$$\sigma_u \simeq \sqrt{\frac{\sum_{n=1}^{N_0} (dt_n - \hat{r}/u)^2 a_n^2}{\sum_{n=1}^{N_0} a_n^2}} \frac{u^2}{\hat{r}} \tag{2}$$

295   If no direct paths exist, i.e. $N_0 = 0$, then the group velocity is computed using the same

296   algorithm for the ray arrivals with one bounce, and so on.

297   Finally, the pseudorange is calculated simply as

$$r_{i,j} = u_{i,j} \Delta t_{i,j} \tag{3}$$

298   This stochastic method for group velocity calculation can run in real-time, appearing to

299   be orders of magnitude faster than general post-processing methods which seek to determine

300   the specific ray itself that best matches a prominent indicator from the arrival structure.

301   The method assumes direct path arrival, where multipath over the shallow receiver depth is

302   trivial for the group velocity calculation; thus we call it the minimal bounce criteria (MBC).

303   The BELLHOP simulation that runs this calculation uses 3600 rays with launch angle fan

304   of -60 to 60 degrees. However, this high density of launch angles creates a greedy estimator

305   of direct path eigenrays, and this simulation pipeline almost always guarantees a direct path

306   found. The MBC improves upon a deterministic estimate in that it considers the simplest

307   ray path, travel time, and amplitude to predict a realistic group velocity.

308 ### 2. *Nearest Bounce Criteria*

309   As shown in the eigenray traces of Fig. 4, an acoustic arrival does not always take

310 the direct path from source to the receiver, and the path it takes is extremely dependent

311 on the sound speed profile. The suggested algorithm, the nearest bounce criteria (NBC),

312 is a slight modification from the minimal bounce criteria, and includes multipath as a new

313 dimension of information with negligible additional computation. This metric was evaluated

314 in post-processing.

315   Given a running estimate for the horizontal group velocity $u_{i,j}$ between nodes i and j,

316 the navigation system has an extrapolated value for range, $\hat{r}$, in the virtual layer, and a

317 recorded travel time, $\Delta t_{i,j}$, in the physical layer. Instead of using only the N_0 rays with

318 neither surface nor bottom bounces to estimate group velocity and subsequently moving to

319 incremental number of bounces only when no valid direct path solutions exist, we solve for

320 the power weighted average of the ray travel time for the N_k rays with k bounces,

$$t_k = \frac{\sum_{n=1}^{N_k} dt_n a_n^2}{\sum_{n=1}^{N_k} a_n^2} \ , \tag{4}$$

321 find the nearest matching power weighted average to recorded travel time,

$$t_{i,j,k} = \min_{k=0,1,2,\dots} |t_k - \Delta t_{i,j}| \tag{5}$$

322 predict a group velocity,

$$u_{i,j} = \frac{\hat{r}}{t_{i,j,k}} \tag{6}$$

323 and estimate the range as was done previously.

$$r_{i,j} = u_{i,j} \Delta t_{i,j} \tag{7}$$

₃₂₄ This method selects a different group velocity based on the multipath arrival structure,

₃₂₅ as the detected arrival is not always the first arrival or the direct path and could even

₃₂₆ be masked by noise or blocked temporarily (Deffenbaugh *et al.*, 1996b). We manually cap

₃₂₇ the number of bounces to 4 because of the smaller operational scale and the attenuation

₃₂₈ accrued with many surface interactions. Bottom bounces are not encoded separately because

₃₂₉ of ray's tendency to refract upward, not due to information limitations. In addition, for a

₃₃₀ more consistent comparison, the local sparse grid is standardized as 11×11 points over 10

₃₃₁ m in range and 20 m in depth, which is similar to those from the vehicle logs. The extra

₃₃₂ size in depth addresses the computational limitations of how time-bounded eigenrays seem

₃₃₃ to stack vertically in the water column, as shown in Fig 4.

₃₃₄ ## III.   REAL-TIME PSEUDORANGE RESULTS

₃₃₅ The modem experiment generated 811 beacon to beacon communication events with their

₃₃₆ own real-time MBC group velocity predictions. As expected, the algorithm is generally

₃₃₇ overestimating range as it resolves a direct path that does not represent the actual arrival.

₃₃₈ This section examines the absolute range error between the pseudorange and the GPS derived

₃₃₉ range with the caveat that the data collected is fairly unbalanced across source depths and

₃₄₀ sound speed conditions.

₃₄₁ Table I breaks down the number of events, mean, median, standard deviation, and maxi-

₃₄₂ mum absolute range error for the *in situ* calculations. The mean and median for both sound

₃₄₃ speeds are similar on the order of centimeters; the chosen weights show a maximum 2 meters

₃₄₄ greater than that of baseline, but it is from a communication event that has no comparison

SSP	Count	Mean [m]	Median [m]	STD [m]	Max [m]
Baseline	243	11.38	11.96	4.23	23.95
Chosen weights	568	11.36	11.40	8.12	26.0

TABLE I. The range estimation error metrics for *in situ* events. The error here is presented as the absolute, not directional, error. Almost all directional errors, however, are positive.

in the baseline data set. Analysis shows that where there is overlap in range between sound speed conditions used for the real-time MBC, the range error difference is no more than a few meters. This is likely driven by the prominence of the duct.

The overarching statistical results show that both sound speed environments, given the smaller operational scales and shallow depths, are accurate enough to approximate the group velocity structure given the local grid. Indeed, the error statistics indicated here are similar to those reported for the ICNN (Randeni *et al.*, 2021) and accurate enough to have facilitated a successful vehicle recovery.

IV.   POST-PROCESSING PSEUDORANGE RESULTS

There are 1242 total beacon to beacon events in the modem experiment that would have been accepted by the ICNN for real-time ranging and navigation had the ranging behavior been running for all modems in the network, and not only for tracking the vehicle. A post-processing analysis that replicated the real-time pipeline was run to overcome the unequal distribution of communication events with respect to depth, range, and sound speed status.

359 It is important to note that the value for the extrapolated range, $\hat{r}$, is only tracked when

360 the modem runs the vehicle behavior; thus we replace $\hat{r}$ with the GPS-tracked range for all

361 modem events. Because $\hat{r}$ converges to the correct solution, a comparison of $\hat{r}$ with the GPS-

362 tracked range shows a normal, zero-centered distribution within the bounds of GPS drift.

363 The present analysis therefore seeds realistic but "omniscient" knowledge of the extrapolated

364 range and leverages the post-processing pipeline to more thoroughly evaluate the acoustic

365 range estimate for all modem events, with three relevant sound speed sources, and both

366 group velocity criterion. Accordingly, the results in this section evaluate the utility of the

367 algorithms and sound speed sources, divorced from their role in the ICNN while maintaining

368 real-time relevance.

A. Group velocity predictions

370 The minimal and nearest bounce algorithms are applied, both without the plane wave

371 extensions, with the three sound speed inputs shown in Fig. 4. The resulting predicted group

372 velocities for a source depth of 30 m are shown in Fig 5. The takeaways from this source

373 depth are representative of those from 20 and 90 m as well (see Supplementary Fig. 10).

374 Because direct path dominates the predictions from the MBC, group velocity estimates

375 are greater than those from NBC. The one instance this is not true is important to men-

376 tion—for a travel time of 2.2 s, where the minimal multipath is dominated by a single bottom

377 bounce (the red line to the furthest transmission in Fig. 4, more detail in Section IV D). The

378 nearest bounce method never classifies anything as direct path for the 30 m source, though

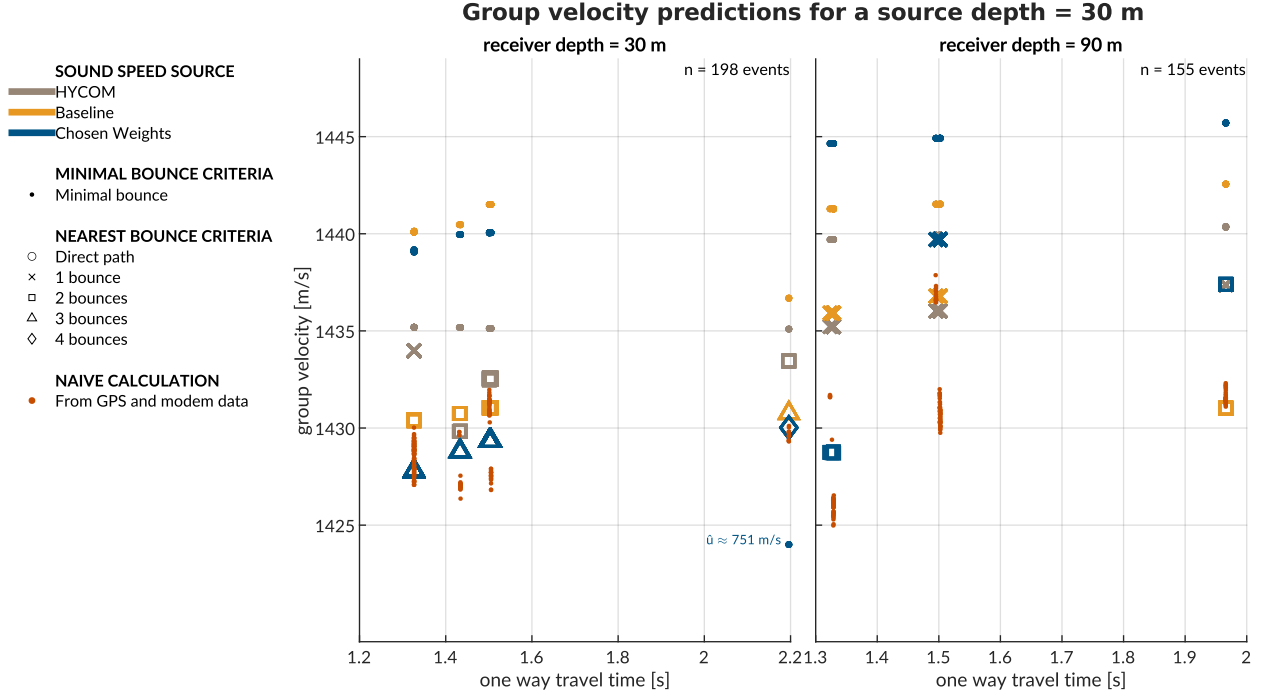379 BELLHOP is quite adept at finding those rays.

FIG. 5. A comparison of group velocity predictions for all beacon to beacon events in post-processing with a source depth of 30 m, with group velocity on the y-axis and recorded travel time on the x-axis. The left panel is for a receiver depth of 30 m; the right panel for 90 m. The sound speed source is indicated by color. The minimal and nearest bounce criterion are distinguished by different marker shapes, compared to the separately colored red dots showing the naive, data-driven group velocity calculation.

The goal of the group velocity estimation is to converge towards the naive group velocity estimation, i.e. the GPS-derived range divided by the recorded travel time. For a 30 m receiver depth, the NBC shows more overlap with data-derived values as it classifies multipath more correctly. For a 90 m receiver depth, the overlap is less accurate due to computational constraints of a limited fan of rays entering the shadow zone rendering a less reliable simulated times of arrival packet.

386 Overall, analysis shows that the higher multipath classification produces more accurate

387 range estimates, likely driven by a tighter bundle of rays. However, that data are too

388 small to draw significant conclusions. Discontinuities in multipath classification verify our

389 hypothesis for its importance to a smoothly varying group velocity, as shown in the cluster

390 for a receiver depth of 30 m, where HYCOM jumps from one to two bounces amidst the

391 baseline SSP and weighted SSP smoothly increasing while consistently seeing two and three

392 bounces, respectively.

B. Pseudorange error versus one way travel time

394 Fig. 6 shows the directional range error footprints for all three sound speed inputs with

395 respect to OWTT, separated by source and receiver depth configurations. The weighted

396 SSP range error generally has the smallest and most zero-centered footprint. The one case

397 it does not is for the source-receiver pairings between 30 and 90 m in depth. The increased

398 error for these reciprocal transmission paths is most likely driven by the computational

399 artifacts encountered when propagating through the steep sound speed gradients of the lens

400 and through the shadow zone. All other source depth pairings are significantly improved

401 using the chosen weights compared to HYCOM or the baseline.

402 When using a linear scaling to convert travel time into range, any offset between the

403 assumed sound speed and the horizontal group velocity produces unconstrained error with

404 increasing receiver distance. Most importantly, we see the consequences of the adaptive

405 group velocity in that range error does not strictly increase with OWTT.

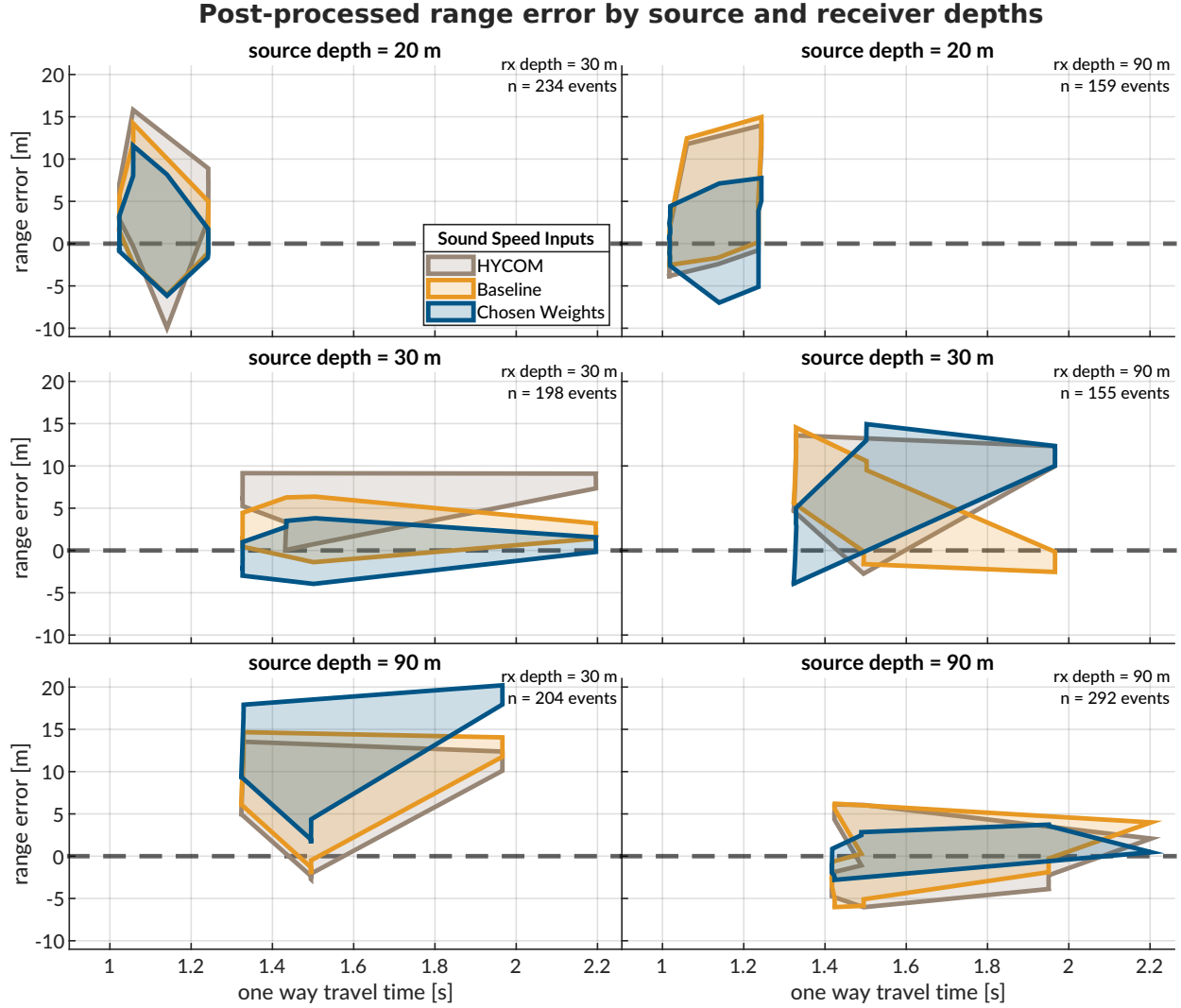**Post-processed range error by source and receiver depths**

FIG. 6. The post-processed range error for source depths of 20, 30, and 90 m, and receiver depths of 30 and 90 m. The dashed gray line shows no error. The shaded region connects the range performance across all events.

C. Pseudorange estimations from the nearest and minimal bounce criteria

The previous section displayed the pseudorange performance using the NBC. Here, we explicitly compare the ranging accuracy between the nearest and minimal bounce criteria for all events in the post-processing pipeline. It is important to note that because the post-

processing pipeline is the same for both methods, that the efficacy of the NBC compared to

the MBC is 100%, as the former simplifies to the latter for direct path classifications.
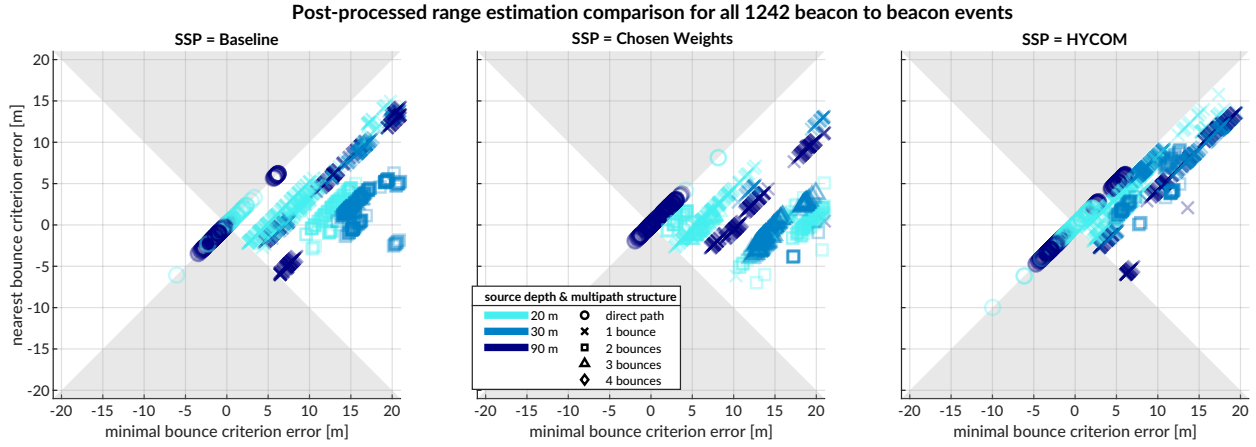
FIG. 7. A comparison of range estimation error for all beacon to beacon events in post-processing. From left to right, the SSPs are the baseline, the chosen weights, and HYCOM. The colors indicate the source depth, darkening with depth, and the shapes indicate the multipath structure. Because this plot is square, the shaded region shows where the updated algorithm is less accurate than the *in situ* algorithm.

Figure 7 is a crossmap for all three SSPs for both group velocity predictors, with the minimal bounce on the x-axis and the nearest bounce on the y-axis; the important range estimation metrics are summarized in table II.

All the events are on the unshaded region of the plots—the MBC has a systemic overestimation, which is reduced via NBC as events straddle the x-axis. The improvement from MBC to NBC is most evident for the realistic sound speed; while the HYCOM SSP improves from a median absolute range error of 6.41 to 4.61 m, the baseline SSP improves from 10.30 to 2.27 m, and the weighted SSP improves from 13.28 to 2.12 m. Table II shows further

statistics on the absolute range error by SSP and group velocity algorithm. The order of magnitude improvement in the ducted SSPs demonstrate the effectiveness of the algorithm exploiting the multipath conditions.

Given the computational constraints of real-time modeling, the gridded approach facilitates enough multipath classification to build in a "ray ensemble" of characteristic group velocities. This result is not always possible when aiming to find eigenrays to just an individual point, even with a higher density of launch angles. An important takeaway for those interested in ray-based localization is leveraging a local grid to give BELLHOP tolerance for finding solutions that otherwise may not be found in a center or single point solution. The limitations of numerical computation, particularly for a complex environment, are more adeptly addressed by accepting some uncertainty in position than by prescribing an exact solution. Even though BELLHOP is a greedy estimator for eigenrays, the additional data created is a negligible burden.

All plots in Fig. 7 show the same 45 degree banding of source depth and multipath structure, indicating systemic GPS noise. The width of those bands indicates the high precision of the acoustic methods relative to lower precision from GPS. Some bands are adjacent to others of the same styling, likely due to ice drift and/or various GPS satellite constellations.

	Baseline		Chosen Weights		HYCOM	
	MBC	NBC	MBC	NBC	MBC	NBC
minimum [m]	0.01	0.00	0.00	0.00	0.11	0.01
25th % [m]	4.96	0.99	6.26	0.95	3.30	2.25
median [m]	10.30	2.27	13.28	2.12	6.41	4.61
75th % [m]	15.81	5.51	19.75	4.11	10.92	7.46
maximum [m]	22.52	14.96	1491	20.21	19.55	15.81

TABLE II. A comparison of range estimation metrics for each sound speed source and group velocity estimation algorithm for all 1283 beacon to beacon events via post-processing. The 0th (minimum), 25th, 50th (median), 75th, and 100th (maximum) percentiles are shown to the range resolution afforded by the WHOI Micro-Modem. There are a few outliers that drive the mean to be higher than the median.

D.   Further analysis of the anomalous beacon to beacon connection

As shown in table II, there is a striking maximum range error of 1491 m for the weighted SSP in the minimal bounce criteria. This section isolates the events that encompass that outlier for further examination, summarized in table III. There are 10 events from South transmitting at 30 m depth to North receiving at 30 m depth. The OWTT spread is from

443 2.1958 to 2.1963 s; the naive group velocity is 1429.3 to 1430.1 m/s; and the GPS-tracked

444 range is from 3138.54 m to 3140.87 m. This example ends up being an excellent case study

445 for how sound speed and multipath fidelity work in concert to minimize range error.

	Baseline		Chosen Weights		HYCOM	
	minimal	nearest	MBC	NBC	minimal	nearest
# bounces	1	3	1	4	0	2
mean OWTT [s]	2.1853	2.1943	4.1812	2.1955	2.1877	2.1902
mean group velocity [m/s]	1436.7	1430.8	750.88	1430.0	1435.1	1433.4
range error [m]	15.4	2.39	-1491	0.77	11.9	8.30

TABLE III. A comparison of range estimation metrics for each sound speed source and group velocity estimation algorithm on all 10 communication events between North at 30 m & South at 30 m.

446 The large error in this instance is driven by the MBC unexpectedly defaulting to a bottom

447 bounce with a much greater OWTT. The NBC classifies the multipath as 4 bounces, reducing

448 the range error from greater than a kilometer to less than a meter. While there is no actual

449 way of knowing if this is the correct multipath structure, the range error is remarkably

450 small, at 0.025%. This pattern of not choosing the minimal observed bounce structure is

451 consistent across all SSPs; the baseline goes from 1 to 3 bounces and HYCOM goes from 0

to 2 bounces. Notably, the baseline and HYCOM range errors are never egregiously large,

but are nonetheless improved with the NBC algorithm. Thus, for acoustically complex

environments, the NBC has a disproportionately positive impact as the estimated SSP

approaches the desired SSP.

E.   GPS sensor drift at polar latitudes

Systemic GPS drift drives the severe banding found in comparisons of range estimations

via both group velocity algorithms, as shown in Fig. 7, with those bands showing 100%

positive correlation between methods and being a similar size in meters. Thus, while this

work is primarily motivated by achieving similar accuracy and precision of GPS, the im-

pressive results from acoustic ranging necessitate a discussion about the limitations of GPS,

particularly at polar latitudes.

The "Global Positioning System Standard Positioning Service Performance Standard",

published by the Department of Defense in Apr 2020 claims that well-designed GPS receivers

have been achieving a horizontal accuracy of 3 meters and a vertical accuracy of 5 meters,

95% of the time. But "well-designed" is an ambiguous enough term that obfuscates two

confounding factors for high latitude GPS drift—operational limitations and ionospheric

scattering.

There are two metrics that demonstrate the operational limitations of GPS tracking

technologies—fix rate and positional dilution of precision (PDOP) (Swanlund *et al.*, 2016).

Fix rate looks at the ratio of successful fixes to overall attempts in acquiring a location. In

animal tracking studies in polar latitudes, fix rates have significantly improved in the last

twenty years, from as low as 26% in 1996 (Moen *et al.*, 1996) to 87.2% in 2018 (Jung *et al.*, 2018). The latter study showed a precision of 4.3 ± 4.0 m and an accuracy of 6.0 ± 4.7 m. While fix rate is a significant metric to evaluate GPS robustness, it is accuracy and precision, and not the fix rate, that explain the severe banding observed; fix rate bias, where various aspects of a landscape can induce bias by impeding the GPS receiver from acquiring its location, is not relevant given the static nature and small time window of ICEX20.

PDOP looks at the effect of satellite geometry on location precision, as satellite orbits are designed to optimize performance for human population density. A high PDOP value indicates a poor geometric configuration, such as satellites being tightly clustered above a GPS receiver, that limits the reliability of trilateration. The literature shows correlation between PDOP values and location error (Swanlund *et al.*, 2016). PDOP is generally thought of as three-dimensional positioning and can be broken down into the horizontal and vertical components, HDOP and VDOP, respectively. The low elevation angles in polar areas are good for horizontal positioning but are susceptible to poorer vertical positioning. Overall this contributes to higher noise level in observations than usually seen in most global applications. The sparse and limited infrastructure in the Arctic make it ideal for satellite-based navigation, with some research proposing new satellite systems to accommodate increased interest in the region (Reid *et al.*, 2016).

However, both of these metrics are functions of the satellite constellation available to any given GPS receiver. The Arctic is beyond the reach of many geostationary satellites, where they are low on the horizon and only visible for brief periods. Given that their positions are tracked by stations on Earth, and their timing is updated twice a day via

495 atomic clock, a reasonable hypothesis for bands of GPS error are different and/or updated

496 satellite connections.

497 The second confounding factor is the ionosphere, the layer of the Earth's atmosphere

498 roughly 80 to 1000 km above the surface that contains a high concentration of ions and

499 free elections. In the ionosphere, electromagnetic signals are affected by the total amount of

500 electrons encountered by the signal; the size of the signal delay is dependent on the carrier

501 frequencies. The literature even references the total amount of electrons encountered by

502 the "GPS raypath" as a means of explaining signal fluctuations (Themens *et al.*, 2015).

503 This variability is observed by seasonal and solar cycle variabilities (Themens *et al.*, 2015),

504 severe ionospheric storms (Mitchell *et al.*, 2005), and auroral activity (increased electron

505 precipitation) (Gwal and Jain, 2011; Jin *et al.*, 2014). In fact, the *aurora borealis* was

506 observed on multiple nights during ICEX20.

507 In a humbling twist, at polar latitudes, GNSS systems experience similar operational,

508 technical, and environmental challenges that we observe in underwater acoustic communi-

509 cations. Figure 8 highlights the GPS and observed OWTT drift relative to the ice move-

510 ment for two pairs of modem buoy connections. The two panels indicate the GPS drift as

511 $\delta R = \sqrt{\delta x^2 + \delta y^2}$ and temporal drift, δt, relative to the median OWTT recorded between

512 the two modems. The dashed line is scaled by a group velocity of 1440 m/s, such that if

513 there were ideal sensor measurements with no drift, all events should exist on or near the

514 line.

515 The top panel shows the connections between the North and East buoys. There is rela-

516 tive, i.e. non-rigid, ice movement between the North and East buoys, evidenced by events
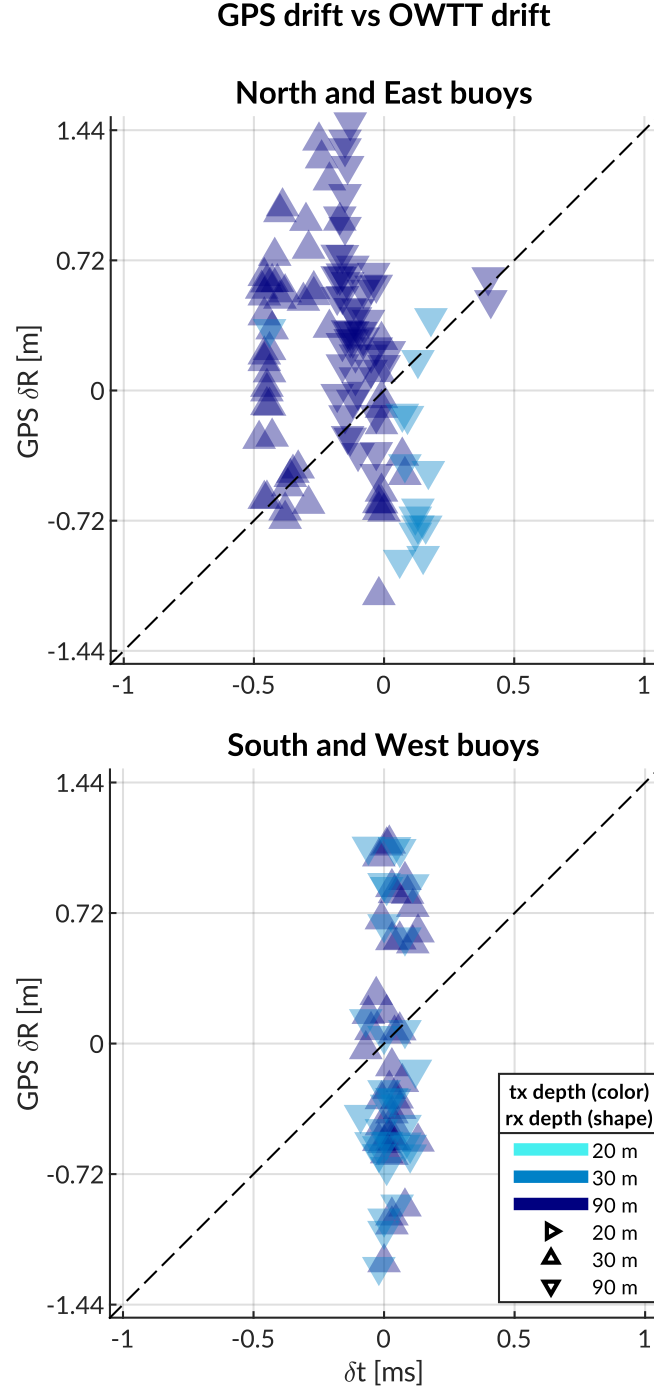
FIG. 8. A comparison of GPS drift (y-axis) versus OWTT drift (x-axis), colored by source and

receiver depth. The physical link between North and East are shown on the top; South and West

is on the bottom.

spanning the dashed line. But the height of the scatter plot is indicative of the precision of

the GPS signal, as it remains consistent across many arrival time bands. Naturally, some

minor offsets between these vertical bands relate to different operational configurations of

source and receiver depth. However, the large majority of events show vertical banding for

the same nominal δt, indicating the amount of GPS drift.

This idea of GPS drift relative to the same OWTT measurements is further indicated by

events between the other two buoys, South and West, in the bottom panel. These buoys are

moving in a more rigid ice floe and there is minimal impact by source and receiver depth

on the spread of OWTT. The GPS drift is much larger relative to the OWTT drift, which

is sensitive to acoustic scattering, multipath, and/or environmental microstructure.

These are just two subsets of the physical links that cover all four GPS modem buoys. The

GPS at camp is the least accurate due to the human activity and infrastructure occluding

the physical puck.

V. DISCUSSION

Underwater navigation research is broadly motivated by acquiring GPS-like navigation

accuracy in GPS-denied conditions. The Arctic, while remote, is the perfect place to test

mature navigation technologies in real GPS-denied conditions.

Range estimation is an essential step of acoustic localization and navigation. Current

approaches in real-time underwater acoustic navigation simplify the non-linear relationship

between a sound speed profile and acoustic propagation with a deterministic sound speed.

Some post-processing approaches attempt to leverage the acoustic arrival structure via var-

ious ray methods, but often use a singular SSP for simplicity, even over long term missions or dynamic conditions. Thus, the conversion from travel time to range, particularly for real-time vehicle deployments, can be pre-conditioned for error growth as the OWTT/range increases.

For GPS-denied navigation, especially in hostile environments like the Arctic, tolerance for error is close to none. This work addresses a critical need in acoustic navigation by retooling acoustic arrival methods generally deemed too complex or labor intensive for real-time, ray-based range estimation to achieve GPS-like positioning.

We hypothesize and validate that the embedded stochastic prediction of a single group velocity is a smoothly varying function of range, source and receiver depth pairings, as well as multipath structure. We employ a GPS-tracked experiment to have a ground truth comparison for real-time localization algorithms. The real-time system achieves GPS-like navigation for an AUV without taking into account multipath structure; the ranging error improves by an order of magnitude with the suggested multipath adaptability, minimizing range error to single meters. Post-processing analysis shows that this method of ranging is sensitive to GPS drift itself; thus embedding a stochastic prediction of the horizontal group velocity has an outsized benefit to minimizing trilateration error.

There are many avenues through which this approach can be further refined and tested for field operations. Amongst them is defining the uncertainty grid for BELLHOP via stochastic or data-driven measures such as the distance traveled by the AUV between ICNN updates or the magnitude of the position corrections by the ICNN. Another is to entirely remove the

seeded range and instead rely on the submerged asset's depth and recorded OWTT to find high probability fields in range.

The literature in underwater acoustic navigation and positioning is either real-time or physics-based. In this paper we demonstrate a field-tested approach that is both real-time and physics-based; this is achieved by coupling data streams with fast acoustic modeling. The methods exploit the upward refracting nature and the total ice cover of the Arctic environment to achieve remarkable ranging accuracy and precision. It transforms multipath, widely considered as an obstacle for acoustic ranging, into a new information content to refine ranging accuracy. We believe that this work enables more accurate range estimation, localization, and/or navigation for any field experiment given known source and receiver depths.

A.   Broader relevance & future work

Performance in other acoustic environments may require introducing a different thresholded metric to sort time of arrivals. Given the NBC algorithm's improvement with increased multipath, its effectiveness is likely only challenged by the valid operational scales of a range independent propagation environment. For mesoscale operations, like that of many gliders, the group velocity criteria may need to be modified to better account for variability driven by range dependent propagation through internal waves, eddies, or even bathymetric changes like underwater volcanoes. BELLHOP simulations provide other relevant eigenray information, like time and angle of arrival, that is ripe for statistical and machine learning methods to classify a representative group velocity. A bespoke and fast ray tracing method,

which was used during ICEX20 to evaluate the acoustic fit of sound speed profile parameterization (Bhatt *et al.*, 2021), can easily report back the number of turning points instead of the number of bounces for multipath classification.

This approach will start to break down in extremely dynamic environments. Fast moving fronts, as seen in estuaries like the Connecticut River into the Long Island Sound, present an entirely new set of challenges not seen by internal waves or eddies. Buoyancy fluctuations in these regions threaten even simple AUV tasks like following a trackline. Acoustic communications are further complicated given a shallow environment with significant scattering (Lavery *et al.*, 2010, 2013; Ross and Lavery, 2012), where fast acoustic modeling may only be coherent for trivial probabilities of the ocean state. Realistic *in situ* considerations of the acoustic environment may not be possible in such environments without complete through-the-sensor integration of echosounder data and/or a hyper-realistic onboard ocean model.

Many approaches to underwater navigation combine it with acoustic tomography, i.e., a joint estimation of both source and receiver locations and the ocean volume between them. There has been considerable success at this effort in post-processing methods, which utilize intensive—and due to the non-linearity of sound propagation, often brute force—computational methods. For vehicle operations, fast tomography is the ideal implementation, in that one can fully consider how sound speed structure, horizontally and vertically, influences sound propagation. AUVs can serve as moving sources to better image the ocean volume (Deffenbaugh, 1997; Elisseeff *et al.*, 2002), where mobile tomography and

navigation converge on the same set of component technologies: position estimation, sound

speed parameterization estimation, ray path identification, and vehicle path optimization.

But there are overwhelming challenges, operationally and computationally, for fast, mobile tomography to become a realistic endeavor. Addressing the spatial and temporal scales of what can be solved deterministically and what must be solved stochastically imposes a resolution constraint on the utility of gridded models—resolving fine features inaccurately (or with a false sense of confidence) could be more harmful than assuming range independence. Given that AUV operations are often on small spatial and temporal scales, the added benefit of a gridded model is quite small, and in cases like the Arctic, may actually mischaracterize the ocean volume. For gliders, with longer and larger operational scales, an ocean model may provide more useful information. Currently gliders are low power and do not have the storage or computational power to run a full-scale, realistic ocean model. A lightweight representation of the key environmental and acoustic features, passed through the same manner of acoustic message from the modem experiment, may drastically improve glider navigation.

The Arctic, a generally inaccessible, dangerous, and expensive region for crewed monitoring via icebreakers, is a prime location to invest in vehicle deployments and underwater observatories (Mikhalevsky *et al.*, 2015). As anthropogenic climate change renders the region more accessible, safe navigation infrastructure and practices will be increasingly vital for industry, tourism, commercial, and military operations. We hope this work enables more frequent and confident monitoring for remote and/or dangerous regions of high climate security importance.

623 **SUPPLEMENTARY FIGURES**

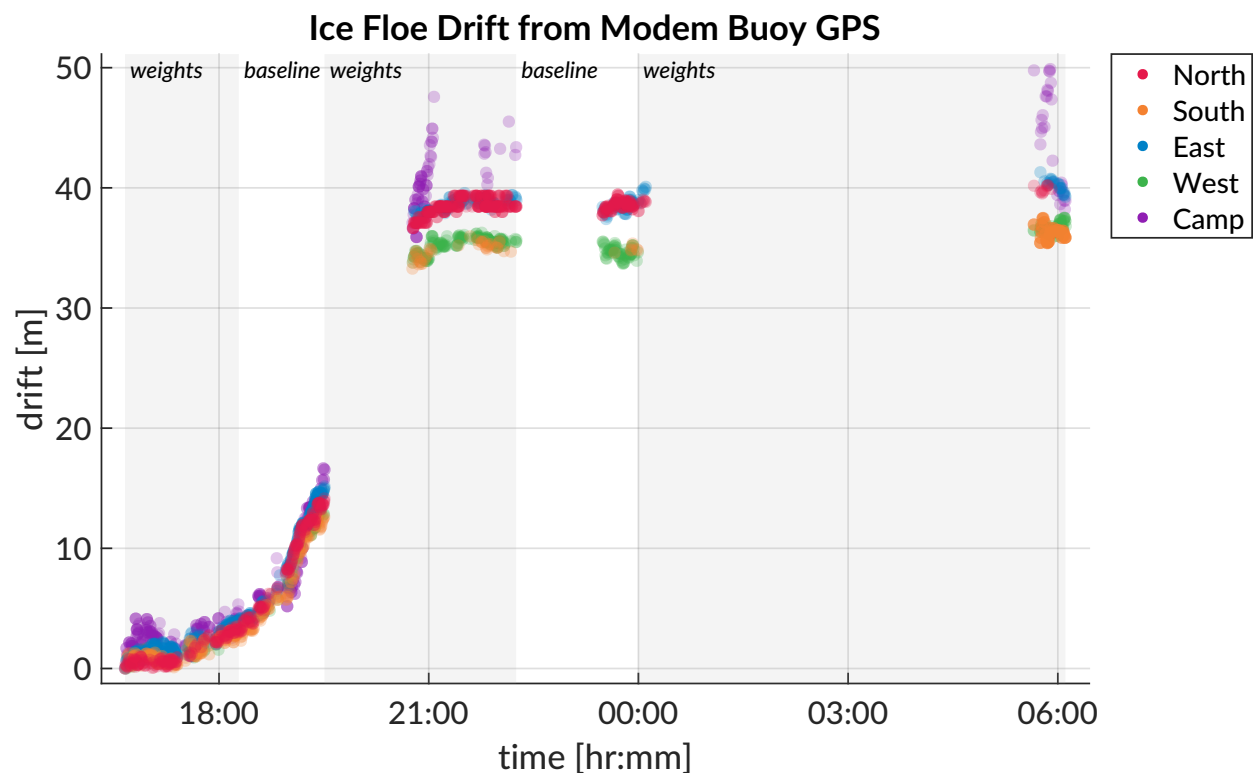624   **Ice movement during the modem experiment**

FIG. 9. The ICNN accounts for ice drift throughout the mission duration. This is the magnitude of the ice drift recorded, at each buoy, throughout the modem experiment. The shaded regions reference which sound speed estimate was used.
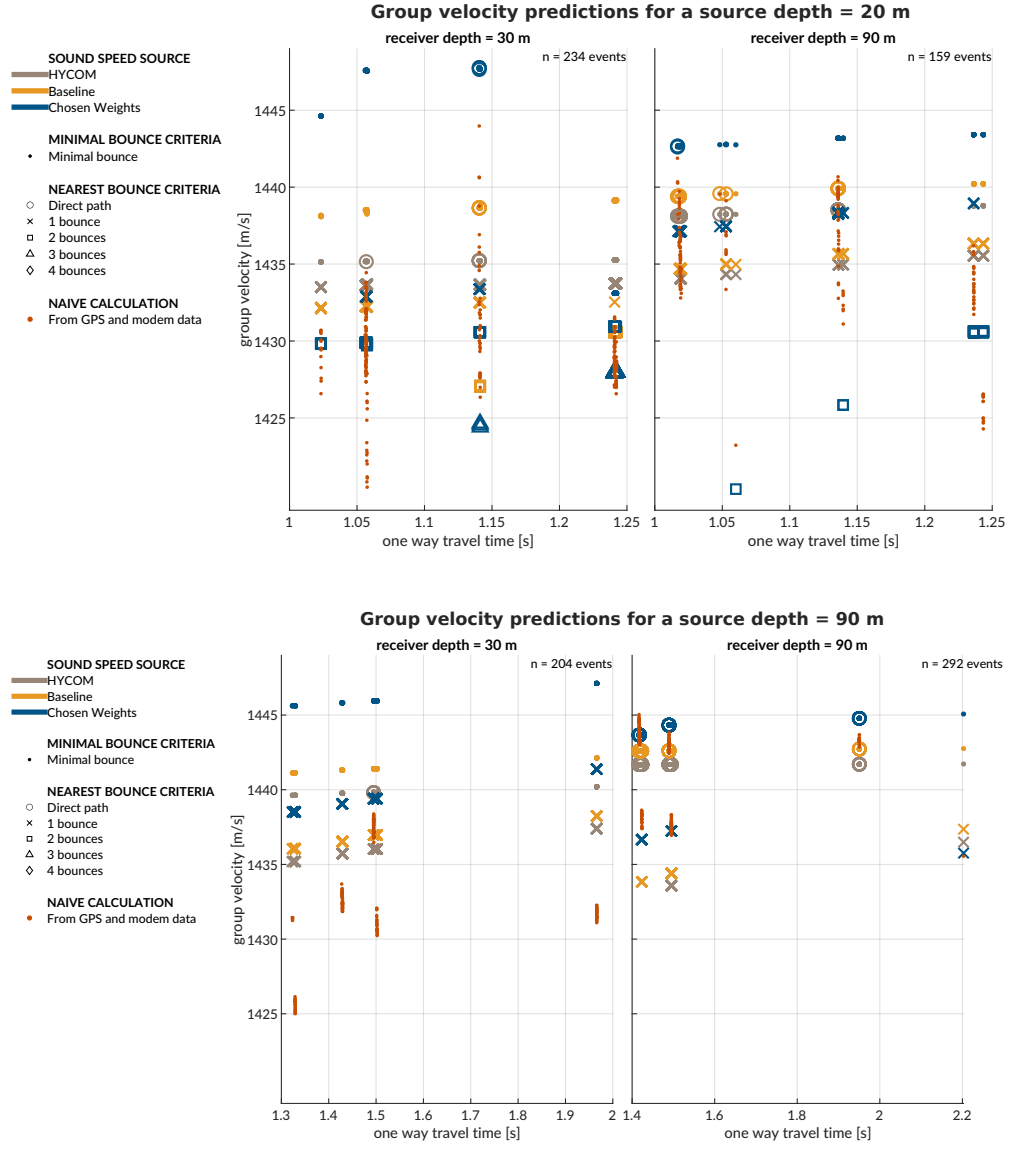
Group velocity prediction by source depth

Group velocity predictions for a source depth = 20 m

Group velocity predictions for a source depth = 90 m

FIG. 10. A comparison of group velocity predictions for all beacon to beacon events in post-processing. The top panel shows a source depth of 20 m; the bottom panel shows a source depth of 90 m. The sound speed source is indicated by color. The minimal and nearest bounce criterion are distinguished by different marker shapes, compared to the separately colored orange dots showing the naive, data-driven group velocity calculation.

ACKNOWLEDGMENTS

Badiey, M., Wan, L., Pecknold, S., and Turgut, A. (**2019**). "Azimuthal and temporal sound fluctuations on the Chukchi continental shelf during the Canada Basin Acoustic Propagation Experiment 2017," The Journal of the Acoustical Society of America **146**(6), EL530–EL536, http://asa.scitation.org/doi/10.1121/1.5141373, doi: 10.1121/1.5141373.

Ballard, M. S., Badiey, M., Sagers, J. D., Colosi, J. A., Turgut, A., Pecknold, S., Lin, Y.-T., Proshutinsky, A., Krishfield, R., Worcester, P. F., and Dzieciuch, M. A. (**2020**). "Temporal and spatial dependence of a yearlong record of sound propagation from the Canada Basin to the Chukchi Shelf," The Journal of the Acoustical Society of America **148**(3), 1663–1680, http://asa.scitation.org/doi/10.1121/10.0001970, doi: 10.1121/10.0001970.

Barker, L. D. L., Jakuba, M. V., Bowen, A. D., German, C. R., Maksym, T., Mayer, L., Boetius, A., Dutrieux, P., and Whitcomb, L. L. (**2020**). "Scientific Challenges and Present Capabilities in Underwater Robotic Vehicle Design and Navigation for Oceanographic Exploration Under-Ice," Remote Sensing **12**(16), 2588, https://www.mdpi.com/2072-4292/

12/16/2588, doi: 10.3390/rs12162588.

Bellingham, J., Leonard, J., Vaganay, J., Goudey, C., Atwood, D., Consi, T., Bales, J., Schmidt, H., and Chryssostomidis, C. (**1993**). "AUV Operations in the Arctic," https://marinerobotics.mit.edu/sites/default/files/Bellingham93uust.pdf.

Bhatt, E. C., Howard, B., and Schmidt, H. (**2021**). "An Embedded Tactical Decision Aid Framework for Environmentally Adaptive Autonomous Underwater Vehicle Communication and Navigation," IEEE Journal of Oceanic Engineering .

Chassignet, E. P., Hurlburt, H. E., Smedstad, O. M., Halliwell, G. R., Hogan, P. J., Wallcraft, A. J., Baraille, R., and Bleck, R. (**2007**). "The HYCOM (HYbrid Coordinate Ocean Model) data assimilative system," Journal of Marine Systems **65**(1), 60–83, https://www.sciencedirect.com/science/article/pii/S0924796306002855, doi: 10.1016/j.jmarsys.2005.09.016.

Deffenbaugh, M. (**1997**). "Optimal Ocean Acoustic Tomography and Navigation with Moving Sources," PhD Thesis, Massachusetts Institute of Technology.

Deffenbaugh, M., Bellingham, J., and Schmidt, H. (**1996**a). "The relationship between spherical and hyperbolic positioning," in *OCEANS 96 MTS/IEEE Conference Proceedings. The Coastal Ocean - Prospects for the 21st Century*, Vol. 2, pp. 590–595 vol.2, doi: 10.1109/OCEANS.1996.568293.

Deffenbaugh, M., Schmidt, H., and Bellingham, J. (**1996**b). "Acoustic positioning in a fading multipath environment," in *OCEANS 96 MTS/IEEE Conference Proceedings. The Coastal Ocean - Prospects for the 21st Century*, Vol. 2, pp. 596–600 vol.2, doi: 10.1109/OCEANS.1996.568294.

Duda, T. F., Zhang, W. G., and Lin, Y.-T. (**2021**). "Effects of Pacific Summer Water layer variations and ice cover on Beaufort Sea underwater sound ducting," Journal of the Acoustical Society of America 21.

Duda, T. F., Zhang, W. G., Lin, Y.-T., and Newhall, A. E. (**2019**). "Long-range sound propagation in the Canada Basin," in *Underwater Acoustics 2019*, https://www.uaconferences.org/docs/2019_papers/UACE2019_976_Duda.pdf.

Elisseeff, P., Schmidt, H., and Xu, W. (**2002**). "Ocean Acoustic Tomography as a Data Assimilation Problem," IEEE Journal of Oceanic Engineering **27**(2), 275–282.

Eustice, R. M., Whitcomb, L. L., Singh, H., and Grund, M. (**2006**). "Recent Advances in Synchronous-Clock One-Way-Travel-Time Acoustic Navigation," in *OCEANS 2006*, pp. 1–6, doi: 10.1109/OCEANS.2006.306931.

Eustice, R. M., Whitcomb, L. L., Singh, H., and Grund, M. (**2007**). "Experimental Results in Synchronous-Clock One-Way-Travel-Time Acoustic Navigation for Autonomous Underwater Vehicles," in *Proceedings 2007 IEEE International Conference on Robotics and Automation*, pp. 4257–4264, doi: 10.1109/ROBOT.2007.364134.

Freitag, L., Ball, K., Partan, J., Koski, P., and Singh, S. (**2015**). "Long range acoustic communications and navigation in the Arctic," in *OCEANS 2015 - MTS/IEEE Washington*, pp. 1–5, doi: 10.23919/OCEANS.2015.7401956.

Gardner, A., and Collins, J. (**2016**). "A second look at Chip Scale Atomic Clocks for long term precision timing," OCEANS 2016 MTS/IEEE Monterey doi: 10.1109/OCEANS.2016.7761268.

Graupe, C. E., van Uffelen, L. J., Webster, S. E., Worcester, P. F., and Dzieciuch, M. A. (**2019**). "Preliminary results for glider localization in the Beaufort Duct using broadband acoustic sources at long range," in *Oceans 2019 MTS/IEEE Seattle*, pp. 1–6, doi: 10.23919/OCEANS40490.2019.8962637.

Gwal, A. K., and Jain, A. (**2011**). "GPS scintillation studies in the arctic region during the first winter-phase 2008 Indian Arctic Expedition," Polar Science **4**(4), 574–587, https://www.sciencedirect.com/science/article/pii/S1873965210001003, doi: 10.1016/j.polar.2010.08.001.

Jakuba, M. V., Roman, C. N., Singh, H., Murphy, C., Kunz, C., Willis, C., Sato, T., and Sohn, R. A. (**2008**). "Long-baseline acoustic navigation for under-ice autonomous underwater vehicle operations," Journal of Field Robotics **25**(11-12), 861–879, https://onlinelibrary.wiley.com/doi/abs/10.1002/rob.20250, doi: https://doi.org/10.1002/rob.20250.

Jin, Y., Moen, J. I., and Miloch, W. J. (**2014**). "GPS scintillation effects associated with polar cap patches and substorm auroral activity: direct comparison," Journal of Space Weather and Space Climate **4**, A23, https://www.swsc-journal.org/articles/swsc/abs/2014/01/swsc140011/swsc140011.html, doi: 10.1051/swsc/2014019.

Jung, T. S., Hegel, T. M., Bentzen, T. W., Egli, K., Jessup, L., Kienzler, M., Kuba, K., Kukka, P. M., Russell, K., Suitor, M. P., and Tatsumi, K. (**2018**). "Accuracy and performance of low-feature GPS collars deployed on bison Bison bison and caribou Rangifer tarandus," Wildlife Biology **2018**(1), https://bioone.org/journals/wildlife-biology/volume-2018/issue-1/wlb.

00404/Accuracy-and-performance-of-low-feature-GPS-collars-deployed-on/10.
2981/wlb.00404.full, doi: 10.2981/wlb.00404.

Kaminski, C., Crees, T., Ferguson, J., Forrest, A., Williams, J., Hopkin, D., and Heard, G.
(**2010**). "12 days under ice – an historic AUV deployment in the Canadian High Arctic,"
in *2010 IEEE/OES Autonomous Underwater Vehicles*, pp. 1–11, doi: 10.1109/AUV.2010.
5779651, iSSN: 2377-6536.

Kepper, J. H., Claus, B. C., and Kinsey, J. C. (**2017**). "MEMS IMU and One-Way-Travel-
Time Navigation for Autonomous Underwater Vehicles," in *Oceans 2017 - Aberdeen*, Ab-
erdeen, UK.

Kucukosmanoglu, M., Colosi, J. A., Worcester, P. F., Dzieciuch, M. A., and Torres, D. J.
(**2021**). "Observations of sound-speed fluctuations in the Beaufort Sea from summer
2016 to summer 2017," The Journal of the Acoustical Society of America **149**(3), 1536–
1548, https://asa.scitation.org/doi/full/10.1121/10.0003601, doi: 10.1121/10.
0003601.

Kukulya, A., Bellingham, J., Kaeli, J., Reddy, C., Godin, M., and Conmy, R. (**2016**).
"Development of a propeller driven long range autonomous underwater vehicle (LRAUV)
for under-ice mapping of oil spills and environmental hazards: An Arctic Domain Center
of Awareness project (ADAC)," in *2016 IEEE/OES Autonomous Underwater Vehicles*
(AUV), pp. 95–100, doi: 10.1109/AUV.2016.7778655, iSSN: 2377-6536.

Kukulya, A., Plueddemann, A., Austin, T., Stokey, R., Purcell, M., Allen, B., Littlefield, R.,
Freitag, L., Koski, P., Gallimore, E., Kemp, J., Newhall, K., and Pietro, J. (**2010**). "Under-
ice operations with a REMUS-100 AUV in the Arctic," in *2010 IEEE/OES Autonomous*

Underwater Vehicles, pp. 1–8, doi: 10.1109/AUV.2010.5779661, iSSN: 2377-6536.

Kunz, C., Murphy, C., Camilli, R., Singh, H., Bailey, J., Eustice, R., Jakuba, M., Naka-mura, K.-i., Roman, C., Sato, T., Sohn, R. A., and Willis, C. (**2008**). "Deep sea underwater robotic exploration in the ice-covered Arctic ocean with AUVs," in *2008 IEEE/RSJ International Conference on Intelligent Robots and Systems*, pp. 3654–3660, doi: 10.1109/IROS.2008.4651097.

Lavery, A. C., Chu, D., and Moum, J. N. (**2010**). "Measurements of acoustic scattering from zooplankton and oceanic microstructure using a broadband echosounder," ICES Journal of Marine Science **67**(2), 379–394, doi: 10.1093/icesjms/fsp242.

Lavery, A. C., Geyer, W. R., and Scully, M. E. (**2013**). "Broadband acoustic quan-tification of stratified turbulence," The Journal of the Acoustical Society of Amer-ica **134**(1), 40–54, http://scitation.aip.org/content/asa/journal/jasa/134/1/10.1121/1.4807780, doi: 10.1121/1.4807780.

LeBlanc, L. R., and Middleton, F. H. (**1980**). "An underwater acoustic sound velocity data model," The Journal of the Acoustical Society of America **67**(6), 2055–2062, https://asa.scitation.org/doi/10.1121/1.384448, doi: 10.1121/1.384448.

Lin, Y., Newhall, A. E., Duda, T. F., Lermusiaux, P. F. J., and Haley, P. J. (**2010**). "Merging Multiple-Partial-Depth Data Time Series Using Objective Empirical Orthogonal Function Fitting," IEEE Journal of Oceanic Engineering **35**(4), 710–721, doi: 10.1109/JOE.2010.2052875.

MacKinnon, J. A., Simmons, H. L., Hargrove, J., Thomson, J., Peacock, T., Alford, M. H., Barton, B. I., Boury, S., Brenner, S. D., Couto, N., Danielson, S. L., Fine, E. C., Graber,

H. C., Guthrie, J., Hopkins, J. E., Jayne, S. R., Jeon, C., Klenz, T., Lee, C. M., Lenn, Y.-D., Lucas, A. J., Lund, B., Mahaffey, C., Norman, L., Rainville, L., Smith, M. M., Thomas, L. N., Torres-Valdés, S., and Wood, K. R. (**2021**). "A warm jet in a cold ocean," Nature Communications **12**(1), 2418, https://www.nature.com/articles/s41467-021-22505-5, doi: 10.1038/s41467-021-22505-5.

McFarlane, J. R., and Mackay, L. (**2015**). "Autonomous Underwater Vehicle operations in the Arctic," in *OCEANS 2015 - MTS/IEEE Washington*, pp. 1–6, doi: 10.23919/OCEANS.2015.7404510.

Mikhalevsky, P. N., Sagen, H., Worcester, P. F., Baggeroer, A. B., Orcutt, J., Moore, S. E., Lee, C. M., Vigness-Raposa, K. J., Freitag, L., Arrott, M., Atakan, K., Beszczynska-Möller, A., Duda, T. F., Dushaw, B. D., Gascard, J. C., Gavrilov, A. N., Keers, H., Morozov, A. K., Munk, W. H., Rixen, M., Sandven, S., Skarsoulis, E., Stafford, K. M., Vernon, F., and Yuen, M. Y. (**2015**). "Multipurpose Acoustic Networks in the Integrated Arctic Ocean Observing System," ARCTIC **68**(5), 11, https://journalhosting.ucalgary.ca/index.php/arctic/article/view/67491, doi: 10.14430/arctic4449.

Mikhalevsky, P. N., Sperry, B. J., Woolfe, K. F., Dzieciuch, M. A., and Worcester, P. F. (**2020**). "Deep ocean long range underwater navigation," The Journal of the Acoustical Society of America **147**(4), 2365–2382, http://asa.scitation.org/doi/10.1121/10.0001081, doi: 10.1121/10.0001081.

Mitchell, C. N., Alfonsi, L., Franceschi, G. D., Lester, M., Romano, V., and Wernik, A. W. (**2005**). "GPS TEC and scintillation measurements from the polar ionosphere during the October 2003 storm," Geophysical Research Letters **32**(12), https://agupubs.

onlinelibrary.wiley.com/doi/abs/10.1029/2004GL021644, doi: https://doi.org/10.1029/2004GL021644.

Moen, R., Pastor, J., Cohen, Y., and Schwartz, C. C. (**1996**). "Effects of Moose Movement and Habitat Use on GPS Collar Performance," The Journal of Wildlife Management **60**(3), 659–668, https://www.jstor.org/stable/3802085, doi: 10.2307/3802085.

Norgren, P., Lubbad, R., and Skjetne, R. (**2014**). "Unmanned underwater vehicles in Arctic operations," p. 14.

Paull, L., Saeedi, S., Seto, M., and Li, H. (**2014**). "AUV Navigation and Localization: A Review," IEEE Journal of Oceanic Engineering **39**(1), 131–149, http://ieeexplore.ieee.org/document/6678293/, doi: 10.1109/JOE.2013.2278891.

Plueddemann, A. J., Kukulya, A. L., Stokey, R., and Freitag, L. (**2012**). "Autonomous Underwater Vehicle Operations Beneath Coastal Sea Ice," IEEE/ASME Transactions on Mechatronics **17**(1), 54–64, doi: 10.1109/TMECH.2011.2174798 conference Name: IEEE/ASME Transactions on Mechatronics.

Porter, M. B. (**2011**). "The BELLHOP Manual and User's Guide (Preliminary Draft)," 1–57, http://esme.bu.edu/data/papers/HLS-2010-1.pdf.

Poulsen, A. J., and Schmidt, H. (**2016**). "Acoustic noise properties in the rapidly changing Arctic Ocean," Buenos Aires, Argentina, p. 070005, http://asa.scitation.org/doi/abs/10.1121/2.0000552, doi: 10.1121/2.0000552.

Randeni, S., Schneider, T., and Schmidt, H. (**2020**). "Construction of a high-resolution under-ice AUV navigation framework using a multidisciplinary virtual environment," in *2020 IEEE/OES Autonomous Underwater Vehicles Symposium (AUV)*, pp. 1–7, doi: 10.

799   1109/AUV50043.2020.9267950.

800   Randeni, S., Schneider, T., Schmidt, H., Bhatt, E., and Viquez, O. (**2021**). "A high-

801   resolution AUV navigation framework with integrated communication and tracking for

802   under-ice deployments," Field Robotics (in review).

803   Reid, T., Walter, T., Blanch, J., and Enge, P. (**2016**). "GNSS Integrity in The Arctic," Nav-

804   igation **63**(4), 469–492, https://onlinelibrary.wiley.com/doi/abs/10.1002/navi.

805   169, doi: https://doi.org/10.1002/navi.169.

806   Ross, T., and Lavery, A. C. (**2012**). "Acoustic scattering from density and sound speed

807   gradients: modeling of oceanic pycnoclines.," The Journal of the Acoustical Society of

808   America **131**(1), EL54–9, http://www.ncbi.nlm.nih.gov/pubmed/22280730, doi: 10.

809   1121/1.3669394.

810   Schmidt, H., and Schneider, T. (**2016**). "Acoustic Communication and Navigation in the

811   New Arctic - A Model Case for Environmental Adaptation," Underwater Communications

812   and Networking (UComms) .

813   Schneider, T., and Schmidt, H. (**2018**). "NETSIM: A Realtime Virtual Ocean Hardware-

814   in-the-loop Acoustic Modem Network Simulator," in *2018 Fourth Underwater Commu-*

815   *nications and Networking Conference (UComms)*, pp. 1–5, doi: 10.1109/UComms.2018.

816   8493188.

817   Schneider, T., Schmidt, H., and Randeni, S. (**2020**). "Self-Adapting Under-Ice Integrated

818   Communications and Navigation Network," in *Underwater Communications*, p. 5.

819   Singh, S., Grund, M., Bingham, B., Eustice, R., Singh, H., and Freitag, L. (**2006**). "Under-

820   water Acoustic Navigation with the WHOI Micro-Modem," in *OCEANS 2006*, IEEE,

Boston, MA, USA, pp. 1–4, http://ieeexplore.ieee.org/document/4099008/, doi: 10.1109/OCEANS.2006.306853.

Stevens, L. A., Straneo, F., Das, S. B., Plueddemann, A. J., Kukulya, A. L., and Morlighem, M. (**2016**). "Linking glacially modified waters to catchment-scale subglacial discharge using autonomous underwater vehicle observations," The Cryosphere **10**(1), 417–432, https://tc.copernicus.org/articles/10/417/2016/, doi: 10.5194/tc-10-417-2016.

Swanlund, D., Maraj, R., Schuurman, N., Hope, R., Donkers, K., Aquin, M., and Rickerby, G. (**2016**). "Gps performance in yukon's arctic coast," Geografiska Annaler: Series A, Physical Geography **98**(4), 361–368, https://doi.org/10.1111/geoa.12143, doi: 10.1111/geoa.12143.

Themens, D. R., Jayachandran, P. T., and Langley, R. B. (**2015**). "The nature of GPS differential receiver bias variability: An examination in the polar cap region," Journal of Geophysical Research: Space Physics **120**(9), 8155–8175, https://agupubs.onlinelibrary.wiley.com/doi/abs/10.1002/2015JA021639, doi: https://doi.org/10.1002/2015JA021639.

Van Uffelen, L. J. V. (**2021**). "Global Positioning Systems: Over Land and Under Sea," Acoustics Today **17**(1), 9.

Webster, S. E., Eustice, R. M., Singh, H., and Whitcomb, L. L. (**2009**). "Preliminary deep water results in single-beacon one-way-travel-time acoustic navigation for underwater vehicles," 2009 IEEE/RSJ International Conference on Intelligent Robots and Systems, IROS 2009 2053–2060, doi: 10.1109/IROS.2009.5354457.

Webster, S. E., Eustice, R. M., Singh, H., and Whitcomb, L. L. (**2012**). "Advances in single-beacon one-way-travel-time acoustic navigation for underwater vehicles," The International Journal of Robotics Research **31**(8), 935–950, https://doi.org/10.1177/0278364912446166, doi: 10.1177/0278364912446166.

Webster, S. E., Freitag, L. E., Lee, C. M., and Gobat, J. I. (**2015**). "Towards real-time under-ice acoustic navigation at mesoscale ranges," in *2015 IEEE International Conference on Robotics and Automation (ICRA)*, pp. 537–544, doi: 10.1109/ICRA.2015.7139231.

Wu, M., Barmin, M. P., Andrew, R. K., Weichman, P. B., White, A. W., Lavely, E. M., Dzieciuch, M. A., Mercer, J. A., Worcester, P. F., and Ritzwoller, M. H. (**2019**). "Deep water acoustic range estimation based on an ocean general circulation model: Application to PhilSea10 data," The Journal of the Acoustical Society of America **146**(6), 4754–4773, https://asa.scitation.org/doi/10.1121/1.5138606, doi: 10.1121/1.5138606.